



HAL
open science

Spin crossover or intra-molecular electron transfer in a cyanido-bridged Fe/Co dinuclear dumbbell: a matter of state

Ie-Rang Jeon, Sergui Calancea, Anangamohan Panja, Dalice M. Piñero Cruz, Evangelia S. Koumoussi, Pierre Dechambenoit, Claude Coulon, Alain Wattiaux, Patrick Rosa, Corine Mathonière, et al.

► To cite this version:

Ie-Rang Jeon, Sergui Calancea, Anangamohan Panja, Dalice M. Piñero Cruz, Evangelia S. Koumoussi, et al.. Spin crossover or intra-molecular electron transfer in a cyanido-bridged Fe/Co dinuclear dumbbell: a matter of state. *Chemical Science*, 2013, 4 (6), pp.2463-2470. 10.1039/C3SC22069A . hal-00822158

HAL Id: hal-00822158

<https://hal.science/hal-00822158>

Submitted on 26 Jul 2022

HAL is a multi-disciplinary open access archive for the deposit and dissemination of scientific research documents, whether they are published or not. The documents may come from teaching and research institutions in France or abroad, or from public or private research centers.

L'archive ouverte pluridisciplinaire **HAL**, est destinée au dépôt et à la diffusion de documents scientifiques de niveau recherche, publiés ou non, émanant des établissements d'enseignement et de recherche français ou étrangers, des laboratoires publics ou privés.

Spin crossover or intra-molecular electron transfer in a cyanido-bridged Fe/Co dinuclear dumbbell: a matter of state†

le-Rang Jeon,^{abcd} Sergiu Calancea,^{cd} Anangamohan Panja,^{cd} Dalice M. Piñero Cruz,^{ab} Evangelia S. Koumoussi,^{abcd} Pierre Dechambenoit,^{ab} Claude Coulon,^{ab} Alain Wattiaux,^{cd} Patrick Rosa,^{cd} Corine Mathonière^{*cd} and Rodolphe Clérac^{*ab}

The design of molecule-based systems displaying tuneable optical and/or magnetic properties under external stimuli has received a great deal of attention in the past few years. This interest is driven by the potential applications in high-performance molecule-based electronics in the areas of recording media, switches, sensors, and displays. As an example, three-dimensional Fe/Co Prussian blue compounds exhibit a concomitant change in magnetic and optical properties due to a temperature- or light-induced metal-to-metal electron transfer. The foregoing remarkable properties in Prussian blues prompted us to design soluble molecular fragments of these coordination networks through a rational building-block approach in order to mimic their properties on a single molecule. With a judicious choice of the ligands for the iron and cobalt molecular precursors, we prepared a dinuclear cyanido-bridged Fe/Co complex that exhibits an unexpected temperature-dependent spin crossover in the solid state while an intramolecular electron transfer triggered by protonation is observed in solution.

DOI: 10.1039/XXXXXXXXXX

Introduction

Since the discovery in 1996 of a reversible thermally and photoinduced metal-to-metal electron transfer in the Prussian blue analogue $K_{0.14}Co[Fe(CN)_6]_{0.71} \cdot 4.93H_2O$,¹ widespread research efforts have been devoted to new cyanido-based materials exhibiting tuneable optical and magnetic properties as a function of external stimuli. This interest is driven in large part by the potential applications of such materials in energy-efficient, switchable molecule-based information storage or electronic devices.^{2–4} Indeed, several attempts to design three-dimensional (3-D) bimetallic cyanido-bridged networks have successfully led to switchable optical and magnetic molecule-based materials.^{5–10} In these network assemblies, it is important

to note that in most of the cases their high dimensionality makes a systematic study of structure–property relationships difficult, and their low solubility limits the shaping of these systems for technological applications.

In this respect, an intense research activity has been recently directed towards molecular fragments of Fe/Co Prussian blues with simple topology and improved solubility. Only in 2004, a molecular $[Fe_2Co_3]$ analogue ($[Co(tmphen)_2]_3\{Fe(CN)_6\}_2$) with $tmphen = 3,4,7,8$ -tetramethyl-1,10-phenanthroline) was reported to show thermally induced intramolecular metal-to-metal electron transfer,^{11,12} although a series of dinuclear complexes and molecular squares involving a $\{Fe(\mu-CN)Co\}$ motif were reported before.^{13–16} Then in 2008, a switchable molecular $[Fe_4Co_4]$ cube, $[{(pzTp)Fe(CN)_3}_4\{Co(pz)_3CCH_2OH\}_4](ClO_4)_4 \cdot 13DMF \cdot 4H_2O$ (with $pzTp =$ tetrapyrazolylborate and $(pz)_3CCH_2OH = 2,2,2$ -tris(pyrazolyl)ethanol), was shown to exhibit both thermally- and photo-induced electron transfer, associated with the transformation of paramagnetic $\{Fe_{LS}^{III}-CN-Co_{HS}^{II}\}$ pairs (LS = low-spin, HS = high-spin) into diamagnetic $\{Fe_{LS}^{II}-CN-Co_{LS}^{III}\}$ pairs exactly like in the family of 3-D Fe/Co Prussian blue analogues.¹⁷ More recently, these magnetic and optical switching properties were also reported in tetranuclear $[Fe_2Co_2]$ squares in the solid state as well as in solution ($[{(L^1)Fe(CN)_3}_2\{Co(L^2)_2\}_2](A)_2 \cdot S$, where L^1 is a trispyrazolylborate derivative and L^2 is a bidentate ligand; A and S are anions and solvents, respectively).^{18–21} The solid-state properties of these $[Fe_2Co_2]$ complexes were transferred into a wide range of

^aCNRS, CRPP, UPR 8641, Pessac, F-33600, France. E-mail: clerac@crpp-bordeaux.cnrs.fr; Fax: +33 5 56 84 56 00; Tel: +33 5 56 84 56 50

^bUniv. Bordeaux, CRPP, UPR 8641, Pessac, F-33600, France

^cCNRS, UPR 9048, ICMCB, Pessac, F-33600, France. E-mail: mathon@icmcb-bordeaux.cnrs.fr; Fax: +33 5 40 00 26 49; Tel: +33 5 40 00 26 82

^dUniv. Bordeaux, ICMCB, UPR 9048, Pessac, F-33600, France

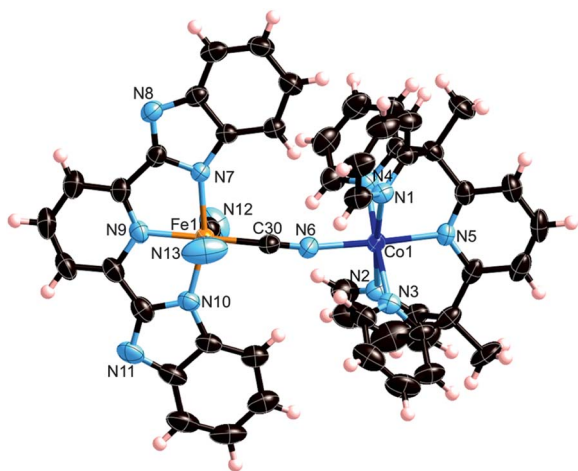


Fig. 1 ORTEP-type view of the dinuclear complex $[(\text{BBP})\text{Fe}(\text{CN})_3\text{Co}(\text{PY5Me}_2)] \cdot 2.5\text{CH}_3\text{OH}$ (**[FeCo]**) at 370 K. The thermal ellipsoids are drawn at the 50% probability level. Yellow, Fe; blue, Co; sky blue, N; black, C; pink, H. Lattice solvent molecules are omitted for clarity.

solvents opening new possibilities to shape this type of molecular switches into more technologically processable systems.²¹ Additionally, the electron transfer mechanism and its associated properties were finely modulated by protonation and the solvent nature.^{20,21} In the past year, additional properties were also found to coexist with the metal-to-metal electron transfer in two new Fe/Co molecular complexes.^{22,23} Indeed, a thermal electron transfer accompanied by switching of the structural polarity was discovered in a trinuclear $[\text{Fe}_2\text{Co}]$ complex ($[\{\text{FeTp}(\text{CN})_3\}_2\text{Co}(\text{Meim})_4]$ with Meim = *N*-methylimidazole),²² while slow relaxation of the magnetization was detected in the photo-excited $[\text{Fe}^{\text{III}}(\text{Co}_2^{\text{II}}\text{Fe}_2^{\text{III}})\text{Fe}^{\text{III}}]$ state of hexanuclear $[\text{Fe}_4\text{Co}_2]$ species ($[\text{Co}_2\text{Fe}_4(\text{H}_2\text{BBP})_2(\text{CN})_6(\mu\text{-CN})_6(\text{pzTp})_4] \cdot 2(1\text{-PrOH}) \cdot 4\text{H}_2\text{O}$ with $\text{H}_2\text{BBP} = 2,6\text{-bis}(\text{benzimidazol-2-yl})\text{pyridine}$).²³

Following this emerging research field, the next challenge is the design of the smallest molecule being able to switch thermally and optically between states using a metal-to-metal electron transfer through a bridging cyanido ligand, in other words a simple dinuclear $[\text{Fe}\text{-CN}\text{-Co}]$ complex. The simplicity of a dinuclear system will allow systematic studies of electron transfer properties depending on the structure and the redox potential of each metal ion, and consequently lead to developing systems with optimized switching properties at a molecular level.

To this end, we have prepared a soluble dinuclear $[\text{Fe}\text{-CN}\text{-Co}]$ fragment of the Fe/Co Prussian blue analogues using organic capping ligands in order to control the dimensionality as well as the magnetic and optical properties. Through spectroscopic studies, electrochemical characterizations, molecular structures and magnetic properties both in the solid state and in solution, this work reports on the first dinuclear molecule able to display two distinct kinds of switching properties.

Results and discussion

To direct the rational formation of a dinuclear cyanido-bridged $[\text{Fe}\text{-CN}\text{-Co}]$ complex, the coordination chemistry of preformed

molecular precursors was exploited. In order to leave only one accessible site on the Co^{II} precursor for the cyanido bridge, a pentadentate ligand, 2,6-bis(1,1-di(pyridin-2-yl)ethyl)pyridine (PY5Me_2), was chosen as a capping ligand.²⁴ For the Fe^{III} precursor, the tridentate planar 2,6-bis(benzimidazol-2-yl)pyridine ligand (H_2BBP) was selected to allow free cyanide groups in a meridional configuration.²⁵ The steric hindrance of both ligands helps in assembling the building blocks in such a way to avoid final compounds with a high dimensional structure, and to shield the desired complex from the neighbouring ones. The stoichiometric reaction of $(\text{Bu}_4\text{N})_2[\text{Fe}(\text{BBP})(\text{CN})_3]$ in methanol (**1**, Fig. S1 and Table S1†) with an acetonitrile solution of $[\text{Co}(\text{PY5Me}_2)(\text{OH}_2)](\text{BF}_4)_2$ (**2**, Fig. S2 and Table S1†) afforded a dinuclear $[\text{Fe}\text{-CN}\text{-Co}]$ complex, $[(\text{BBP})\text{Fe}(\text{CN})_3\text{Co}(\text{PY5Me}_2)] \cdot 2.5\text{CH}_3\text{OH}$ in high yield (**[FeCo]**). **[FeCo]** successfully crystallizes as a neutral species in the monoclinic $P2_1/c$ space group (see Fig. 1 and Table S2†).

As expected, one of the cyanide groups on the Fe-precursor is coordinated to the axial position of the Co-precursor to give the desired $\{\text{Fe}(\mu\text{-CN})\text{Co}\}$ motif. At 370 K, average Co-N and Fe-C bond lengths are 2.108(3) Å and 1.943(4) Å, respectively (Table S3†). These values are in close agreement with those expected for $\text{Co}^{\text{II}}_{\text{HS}}$ and $\text{Fe}^{\text{III}}_{\text{LS}}$ ions, considering the valence bond sum analysis and charge compensation.^{17–23} In the crystal, the complexes are stabilized through $\pi\text{-}\pi$ interactions along the crystallographic *a* direction and $\sigma\text{-}\pi$ interactions in the *ab* plane (Fig. S5 and S6†).

The magnetic susceptibility, χ , of **[FeCo]** was measured and is plotted as a χT vs. *T* plot in Fig. 2. The “S”-shaped curve observed around 220 K could be the signature of an electron transfer process. The high temperature (360 K) χT value is close to the $3.1 \text{ cm}^3 \text{ K mol}^{-1}$ expected for the sum of the $\text{Fe}_{\text{LS}}^{\text{III}}$ ($S = 1/2$, $g = 2.26$ obtained for **1**) and $\text{Co}_{\text{HS}}^{\text{II}}$ ($S = 3/2$, $g = 2.36$ obtained for **2**) centres. Nevertheless, an Fe-Co electron

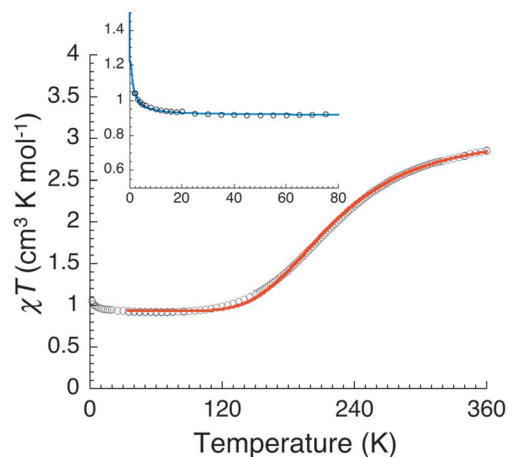


Fig. 2 Temperature dependence of the χT product of **[FeCo]**. χ is the molar magnetic susceptibility that is equal to M/H . Experimental data (black circles) were collected in an applied field of 1000 Oe and the red solid line represents the best fit based on an ideal solution model.^{†29} Inset, zoom of low temperature region. Data were fitted (blue line) by the theoretical susceptibility deduced from the Heisenberg dinuclear isotropic spin Hamiltonian: $H = -2J S_{\text{Co}} S_{\text{Fe}}$.

transfer should involve the transformation of a paramagnetic $\{\text{Fe}_{\text{LS}}^{\text{III}}\text{-CN-Co}_{\text{HS}}^{\text{II}}\}$ pair into a diamagnetic $\{\text{Fe}_{\text{LS}}^{\text{II}}\text{-CN-Co}_{\text{LS}}^{\text{III}}\}$ pair, while a significant χT value ($0.93 \text{ cm}^3 \text{ K mol}^{-1}$) is measured below 100 K. In order to clarify whether this thermal behaviour is due to a partial electron transfer process or another phenomenon involving a change of electronic states, additional crystallographic data were collected at 90 K.

At a first look, the temperature does not have a notable effect on the structure (at 90 and 370 K, $[\text{FeCo}]$ crystallizes in the same $P2_1/c$ space group), unit-cell parameters and average bond distances (Fig. S4, Tables S2 and S3†). Nevertheless, significant differences are seen on individual Co–N bonds and in the geometry of the cobalt coordination sphere. A remarkable elongation of the Co1–N1 and Co1–N2 bonds is observed at 90 K with values of 2.242(3) Å and 2.228(3) Å, respectively (from 2.191(2) Å and 2.182(3) Å at 370 K), while all other Co–N bond lengths decrease by about 0.1 Å. Consequently, the $\{\text{Fe}(\mu\text{-CN})\text{Co}\}$ unit becomes more linear, as evidenced by the evolution of the Co–N6–C30 angle from 168.2(3)° at 370 K to 172.0(3)°. The resulting strong distortion of the Co coordination geometry corresponds to the Jahn–Teller effect for a Co^{II} low spin state induced by the presence of a single electron in e_g orbitals, as observed in many examples of Co^{II} spin crossover complexes.^{26,27} Those features and the unaffected Fe coordination sphere with temperature suggest a thermal spin crossover on the Co^{II} ion rather than an electron-transfer phenomenon within the Fe–Co pair.

In order to further support the unexpected Co^{II} spin crossover scenario in $[\text{FeCo}]$, ^{57}Fe Mössbauer studies were performed at 298 and 4.2 K. As shown in Fig. 3, a quadrupole doublet characteristic for $\text{Fe}_{\text{LS}}^{\text{III}}$ was observed at 4.2 K (with $\delta = 0.002 \text{ mm s}^{-1}$ and $\Delta E_{\text{Q}} = 2.99 \text{ mm s}^{-1}$; δ being the isomer shift and ΔE_{Q} the quadrupole splitting).²⁸ As the temperature was raised to 298 K, the same $\text{Fe}_{\text{LS}}^{\text{III}}$ doublet was observed with $\delta = -0.052 \text{ mm s}^{-1}$ and $\Delta E_{\text{Q}} = 2.96 \text{ mm s}^{-1}$, showing that the Fe electronic state remains unchanged. This Mössbauer study confirms thus the absence of a thermal intramolecular electron-transfer process occurring between Co^{II} and Fe^{III} in the solid state for $[\text{FeCo}]$.

The Co^{II} spin crossover in $[\text{FeCo}]$ is also supported by the magnetic properties (Fig. 2) that are in agreement with an $[\text{Fe}_{\text{LS}}^{\text{III}}\text{-CN-Co}_{\text{LS}}^{\text{III}}]$ ground state below 100 K and an $[\text{Fe}_{\text{LS}}^{\text{III}}\text{-CN-Co}_{\text{HS}}^{\text{II}}]$ excited state thermally populated above 100 K. At 360 K, the χT product is not reaching a well-defined plateau but measurements at higher temperatures unfortunately led to an irreversible alteration of $[\text{FeCo}]$ induced by the loss of the interstitial solvent molecules, confirmed by thermogravimetric analysis (Fig. S8†). Nevertheless as routinely done for spin crossover systems, χT vs. T data were well fitted between 25 and 360 K to an ideal solution model† (Fig. 2)²⁹ with $\chi T_{\text{LS}} = 0.94(1) \text{ cm}^3 \text{ K mol}^{-1}$, $\chi T_{\text{HS}} = 3.19(4) \text{ cm}^3 \text{ K mol}^{-1}$, $T_{1/2} = 228(2) \text{ K}$ and $\Delta H = 9.2(2) \text{ kJ mol}^{-1}$. The χT_{LS} and χT_{HS} values for the low and high temperature states correspond well to the expected ones for $[\text{Fe}_{\text{LS}}^{\text{III}}\text{-CN-Co}_{\text{LS}}^{\text{III}}]$ and $[\text{Fe}_{\text{LS}}^{\text{III}}\text{-CN-Co}_{\text{HS}}^{\text{II}}]$ pairs respectively ($\text{Fe}_{\text{LS}}^{\text{III}}$: $S = 1/2$, $g \approx 2.26$; $\text{Co}_{\text{LS}}^{\text{III}}$: $S = 1/2$, $g \approx 2.19$ and $\text{Co}_{\text{HS}}^{\text{II}}$: $S = 3/2$, $g \approx 2.36$). Furthermore, it is worth noting that the enthalpy and entropy changes, ΔH and $\Delta S = \Delta H/T_{1/2} = 40(1) \text{ J}$

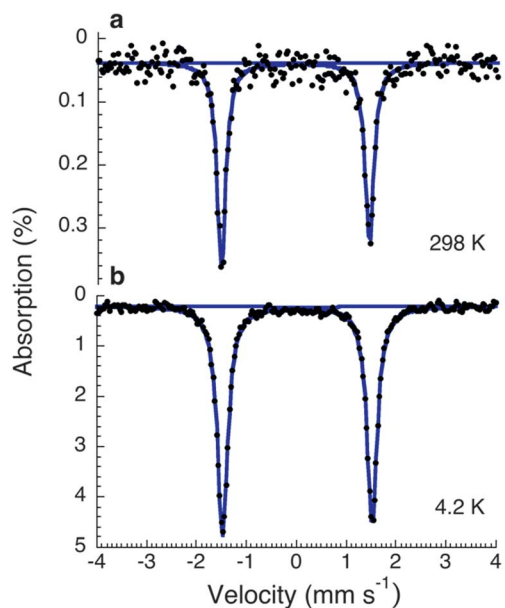


Fig. 3 ^{57}Fe Mössbauer spectra of $[\text{FeCo}]$ collected at 298 K (a) and at 4.2 K (b). The dark points correspond to experimental data, and the blue lines represent the spectral simulation for a $\text{Fe}_{\text{LS}}^{\text{III}}$ ion with the following parameters, $\delta = -0.052 \text{ mm s}^{-1}$ and $\Delta E_{\text{Q}} = 2.96 \text{ mm s}^{-1}$ at 298 K (a), and $\delta = 0.002 \text{ mm s}^{-1}$ and $\Delta E_{\text{Q}} = 2.99 \text{ mm s}^{-1}$ at 4.2 K (b).

$\text{K}^{-1} \text{ mol}^{-1}$, are well in the range for a Co^{II} spin crossover.²⁶ Decreasing the temperature below 20 K, the small increase of the χT product evidences for the first time a ferromagnetic interaction, J , between $\text{Fe}_{\text{LS}}^{\text{III}}$ ($S_{\text{Fe}} = 1/2$) and $\text{Co}_{\text{LS}}^{\text{II}}$ ($S_{\text{Co}} = 1/2$) centres through a cyanido bridge (see Fig. 2). This exchange coupling was estimated at $+0.68(9) \text{ K}$ from the fitting of the experimental data below 80 K (with $g_{\text{av}} = 2.21(5)$) on the basis of a dinuclear Heisenberg spin Hamiltonian.‡ As a consequence of this intramolecular ferromagnetic interaction, the dinuclear $[\text{FeCo}]$ complex possesses an $S_{\text{T}} = 1$ spin ground state.

This detailed study allows us to conclude that, to the best of our knowledge, $[\text{FeCo}]$ is the only known complex exhibiting a cobalt(II) spin crossover in a heterobimetallic system.

The absence of intra-molecular electron transfer in the solid-state prompted us to study the properties of this complex in solution. Very recently, our team, as well as Oshio's group, studied in solution the electron-transfer process of $[\text{Fe}_2\text{Co}_2]$ complexes for the possibility of fine-tuning its characteristics such as $T_{1/2}$.^{20,21} Solubility and stability tests led to the conclusion that $[\text{FeCo}]$ is only significantly soluble in DMSO (dimethyl sulfoxide).¶ Therefore DMSO solutions of $[\text{FeCo}]$ were prepared to examine whether potential electron-transfer properties could be favoured by the solvent and/or protonation. The possibility of thermal spin crossover or electron-transfer processes in DMSO solution was tested by magnetic susceptibility measurements, but only the paramagnetic $[\text{Fe}_{\text{LS}}^{\text{III}}\text{-CN-Co}_{\text{HS}}^{\text{II}}]$ species was detected over all the experimental temperature range (Fig. S9†).

To examine the effect of protonation, UV-vis absorption spectra were measured upon addition of trifluoroacetic acid (TFA) to a DMSO solution of $[\text{FeCo}]$. Upon acid addition, a significant spectrum modification is evidenced by a colour

change of the solution from dark green to purple (Fig. 4a). The intense absorption at $14\,800\text{ cm}^{-1}$ before acid addition can be attributed to ligand-to-metal charge transfer (LMCT) for the $\{(\text{BBP})\text{Fe}^{\text{III}}(\text{CN})_3\}$ part of the $[\text{FeCo}]$ complex based on the UV-vis spectra of **1** that exhibits a very similar (in shape and intensity) LMCT band at $16\,100\text{ cm}^{-1}$ (Fig. S10†).^{20,30a,b} As the TFA amount increases, the intensity of this $\{(\text{BBP})\text{Fe}^{\text{III}}(\text{CN})_3\}$ LMCT band vanishes, and a new absorption band appears at $18\,700\text{ cm}^{-1}$ (Fig. 4a). It is worth mentioning here that the presence of a seemingly isosbestic point at $17\,390\text{ cm}^{-1}$ might indicate that only two species are involved in the observed process. Nevertheless, the two curves representing the normalized absorbance variation at $14\,800\text{ cm}^{-1}$ and $18\,700\text{ cm}^{-1}$ upon acid addition (Fig. 4b) display an asymmetric evolution, with the crossing point not located at 0.5, therefore demonstrating the presence of more than two species in solution (*vide infra*).

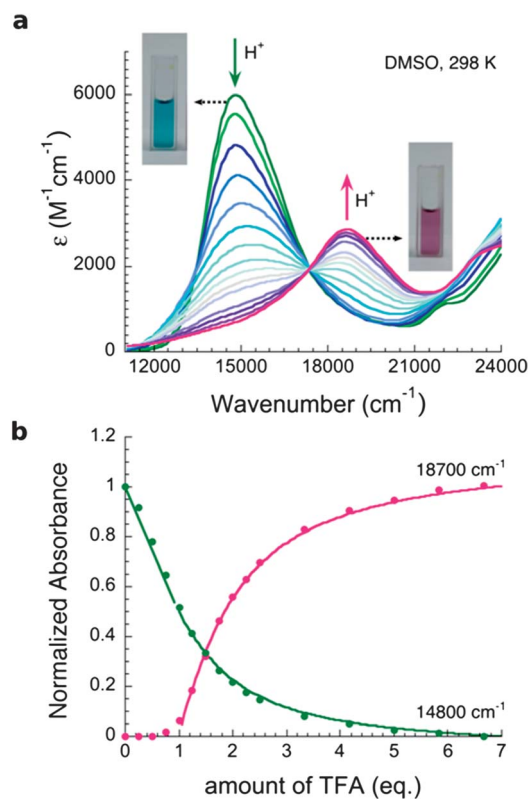


Fig. 4 UV-vis spectroscopic characterization of $[\text{FeCo}]$ in DMSO solution at 298 K. (a) Spectral evolution upon TFA addition to a $[\text{FeCo}]$ DMSO solution ($2.68 \times 10^{-4}\text{ M}$; note that there is no additional band down to 5000 cm^{-1}). From green to purple, the acid addition is increasing with an interval of (i) 0.25 eq. up to 2.5 eq., and (ii) 0.84 eq. up to 6.7 eq. (b) The normalized absorbance of each characteristic band: dark green for $14\,800\text{ cm}^{-1}$ and purple for $18\,700\text{ cm}^{-1}$. The solid lines after the first equivalence point (TFA > 1 eq.) are the results of the acid-base titration modelling (see ESI†). Before the first equivalence point (TFA \leq 1 eq.), the UV-vis spectra is not modified around $18\,700\text{ cm}^{-1}$ (purple curve) demonstrating the absence of di-protonated $[\text{H}_2\text{FeCo}]^{2+}$ species and thus that all added protons produce only mono-protonated $[\text{HFeCo}]^+$ species. The linear variation of the green curve confirms this result and furthermore, its slope of -0.5 indicates that the absorbance of the mono-protonated complex is twice weaker than the non-protonated one (the observed slope would be 0 if the two species had the same absorbance).

To probe if the observed process is possibly linked to an intramolecular electron transfer and spin-state changes in solution upon TFA addition, $[\text{FeCo}]$ ^1H NMR was measured in deuterated-DMSO (d-DMSO), before and after adding an excess of deuterated-TFA (d-TFA; 10 eq.). The untreated solution showed paramagnetic shifts of all resonances as expected for a paramagnetic $[\text{Fe}_{\text{LS}}^{\text{III}}\text{-CN-Co}_{\text{HS}}^{\text{II}}]$ species. The resonance peaks could be attributed to each ligand as shown in Fig. 5, based on ^1H NMR and ^1H - ^1H COSY measurements of **1**, **2** and $[\text{FeCo}]$ (Fig. S11, S12 and S13†). In contrast, the purple-coloured solution after treatment with d-TFA did not show any paramagnetic shifts, and all resonances could be assigned perfectly to the PY5Me₂ and BBP ligands in a 1 : 1 ratio (Figs. S14 and S15†). The NMR data unambiguously demonstrate the presence in solution of a diamagnetic species that can only be the $[\text{Fe}_{\text{LS}}^{\text{II}}\text{-CN-Co}_{\text{LS}}^{\text{III}}]$ complex resulting from an electron transfer process triggered by acid addition. Therefore the characteristic absorption observed at $18\,700\text{ cm}^{-1}$ (Fig. 4) should be a metal-to-ligand charge transfer (MLCT) band^{30a,c,d} for the $\text{Fe}^{\text{II}}/\text{BBP}$ part of the fully protonated $[\text{FeCo}]$ complex. This conclusion is well supported by the UV-vis spectrum of the fully protonated reduced form of **1** that exhibits a characteristic MLCT band at 17800 cm^{-1} (Fig. S10†).^{30c,d} Those results evidence the occurrence of an intramolecular electron transfer induced by the protonation in DMSO solution of $[\text{FeCo}]$: upon controlled proton addition, the paramagnetic $[\text{Fe}_{\text{LS}}^{\text{III}}\text{-CN-Co}_{\text{HS}}^{\text{II}}]$

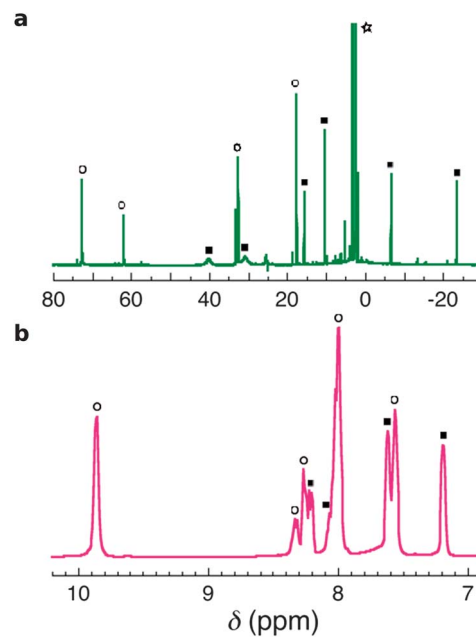


Fig. 5 ^1H NMR spectra of $[\text{FeCo}]$ in d-DMSO solutions at 298 K. (a) The paramagnetic $[\text{Fe}_{\text{LS}}^{\text{III}}\text{-CN-Co}_{\text{HS}}^{\text{II}}]$ species is present in the solution before the treatment with d-TFA (note that this spectrum is not the sum of the precursor spectra shown in Fig. S11† demonstrating the non-dissociation of the complex in DMSO). (b) The diamagnetic $[\text{Fe}_{\text{LS}}^{\text{II}}\text{-CN-Co}_{\text{LS}}^{\text{III}}]$ species is detected after the addition of 10 eq. of d-TFA. Empty circles indicate the resonances from PY5Me₂ ligand coordinated to the cobalt ion, and full squares are those from BBP ligand coordinating the iron centre. The intense peaks marked with an empty star are from the solvents, H₂O and DMSO.

complex is progressively converted into a diamagnetic $[\text{Fe}_{\text{LS}}^{\text{II}}\text{-CN-Co}_{\text{LS}}^{\text{III}}]$ species.

Additional experimental evidence on the protonation-induced electron transfer in $[\text{FeCo}]$ solutions is given by cyclic voltammetry experiments (Fig. 6). Before any acid addition to a DMSO solution of $[\text{FeCo}]$, two reversible redox waves were detected for $\{\text{Fe}^{\text{III}}\text{Co}^{\text{II}}/\text{Fe}^{\text{II}}\text{Co}^{\text{II}}\}$ and $\{\text{Fe}^{\text{III}}\text{Co}^{\text{III}}/\text{Fe}^{\text{III}}\text{Co}^{\text{II}}\}$ couples at -0.91 V and 0.01 V, respectively (Fig. 6a).[¶] After adding 0.8 eq. of acid (Fig. 6b), the former wave almost vanished, while the latter remained almost unaffected, and concomitantly, a new reversible redox wave appeared at -0.39 V. This result implies that the proton addition significantly affects the redox properties of the Fe site and not those of the Co part. This behaviour was confirmed by the redox properties of **1** and **2** upon acid addition (Fig. S16[†]). Independently of TFA addition, the Co precursor, **2**, showed at $+0.13$ V a reversible one-electron redox wave corresponding to the $\text{Co}^{\text{III}}/\text{Co}^{\text{II}}$ couple. The redox properties of **2** are thus not modified by protonation as observed for the Co part of $[\text{FeCo}]$. In contrast, the redox potential of the Fe precursor, **1**, is drastically changed upon proton addition: from -1.05 V without acid, up to -0.46 V for 3 eq. of TFA. Fortunately, the diprotonated paramagnetic complex, $[\text{Fe}^{\text{III}}(\text{H}_2\text{BBP})(\text{CN})_3]\cdot 2\text{H}_2\text{O}$ (**3**) was crystallized (see Experimental section) and revealed that the two protons are positioned on the imine nitrogens of the BBP benzimidazole groups (Fig. S3[†]). In addition as shown by cyclic voltammetry experiments, the redox $\text{Fe}^{\text{III}}/\text{Fe}^{\text{II}}$ potential for **3** (Fig. S17[†]) corresponds well to the one observed for **1** after adding two equivalents of acid. The aforementioned results strongly suggest that, by adding acid to the $[\text{FeCo}]$ solution, protonation occurs rather on the BBP ligand than on the free cyanides as proposed by other groups for related systems.^{20,31} Consequently, these nitrogen atoms in **1**, and thus in $[\text{FeCo}]$, act as weak bases, and their protonation results in the positive shift of the $\text{Fe}^{\text{III/II}}$ redox potential. Keeping

in mind that the electron transfer is governed by the redox potential difference (ΔE) between metal ion sites,³² it is worth noting that ΔE between Co and Fe metal centres is strongly reduced after the protonation, as illustrated by $[\text{FeCo}]$ as well as by **1**, **2** and **3**. Only at around 1 eq. of acid addition to $[\text{FeCo}]$, two new reversible redox waves appear progressively at -0.45 V and -0.26 V (Fig. 6c and d). Given the fact that the diamagnetic $\{\text{Fe}^{\text{II}}\text{Co}^{\text{III}}\}$ species is present in solution after the acid treatment as shown by the NMR study (Fig. 5b), the two redox waves can be straightforwardly attributed to $\{\text{Fe}^{\text{II}}\text{Co}^{\text{III}}/\text{Fe}^{\text{II}}\text{Co}^{\text{II}}\}$ and $\{\text{Fe}^{\text{III}}\text{Co}^{\text{III}}/\text{Fe}^{\text{II}}\text{Co}^{\text{III}}\}$ couples, respectively. Thus, the redox waves corresponding to the cobalt and iron sites are inverted after protonation as expected for a complex experiencing an electron transfer process. This study demonstrates that the protonation of the BBP ligand decreases ΔE between the Fe and Co centres, and consequently, induces an electron transfer process in the final system as evidenced by the inversion of redox waves.

The reaction mechanism of the $[\text{FeCo}]$ protonation in solution was investigated from a theoretical point of view, assuming the possibility of a double protonation of this complex. Thus, three possible species are present in solution: the non-protonated $[\text{FeCo}]$, the mono-protonated $[\text{HFeCo}]^+$, and the di-protonated $[\text{H}_2\text{FeCo}]^{2+}$ complexes. The reaction scheme was described as acid-base titration, and the obtained model (see ESI[†]) was used to reproduce the dependence of the normalized absorbances upon acid addition. An excellent theory/experience agreement (Fig. 4b and S18[†]) is obtained leading to the following results: (i) $[\text{HFeCo}]^+$ is produced prior to the di-protonated one, since $[\text{HFeCo}]^+$ (estimated $\text{p}K_{\text{A}2} = 6.42$) is a weaker acid than $[\text{H}_2\text{FeCo}]^{2+}$ (estimated $\text{p}K_{\text{A}1} = 4.17$). Therefore, the introduced protons produce only $[\text{HFeCo}]^+$ until the initial $[\text{FeCo}]$ is consumed. This result explains well the cyclic voltammetry data (appearance of the two new reversible redox waves at -0.45 V and -0.26 V only around 1 eq. of acid addition to $[\text{FeCo}]$) and also why the normalized intensity of the $18\,700\text{ cm}^{-1}$ absorption band (proportional to the $[\text{H}_2\text{FeCo}]^{2+}$ concentration) stays at almost zero up to adding 1 eq. of acid (as similarly observed for the Fe precursor, Fig. S19[†]). (ii) The $14\,800\text{ cm}^{-1}$ absorption band can be attributed to both $[\text{FeCo}]$ and $[\text{HFeCo}]^+$ species. Consequently, $[\text{HFeCo}]$ shows the characteristic LMCT band of the Fe^{III} site at a similar energy to $[\text{FeCo}]$ (as observed for **1**, Fig. S19[†]), allowing the existence of an isosbestic point. These observations and model provide a full explanation of the UV-vis spectral changes upon protonation. Three different species are involved, explaining the asymmetric shape of the normalized absorption evolution upon proton addition. Furthermore, the diamagnetic species created by intramolecular electron transfer upon protonation is the di-protonated $[\text{H}_2\text{Fe}_{\text{LS}}^{\text{II}}\text{Co}_{\text{LS}}^{\text{III}}]^{2+}$ complex.

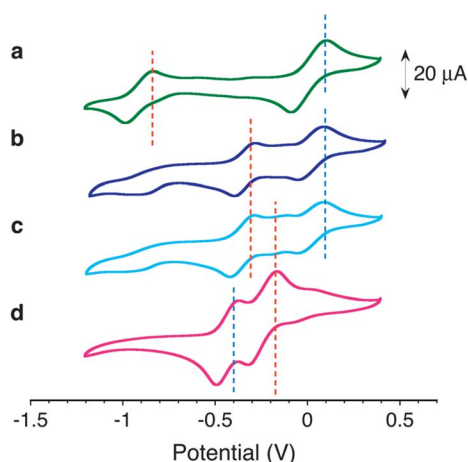


Fig. 6 Cyclic voltammogram of $[\text{FeCo}]$ in DMSO solutions (≈ 1 mM). Collected in a 0.1 M solution of $\text{Bu}_4\text{N}(\text{PF}_6)$ in DMSO with a scan rate of 0.1 V s^{-1} . Potentials were referenced to the $[\text{Cp}_2\text{Fe}]^{1+/0}$ couple: (a) as prepared; (b) after 0.8 eq. of TFA; (c) after 1 eq. of TFA; and (d) after 4 eq. of TFA. For an easy comparison, red and blue dashed lines indicate the maximum of the characteristic oxidation waves of Fe and Co centres, respectively.

Conclusion

A new cyanido-bridged dinuclear $[(\text{BBP})\text{Fe}(\text{CN})_3\text{Co}(\text{PY5Me}_2)]\cdot 2.5\text{CH}_3\text{OH}$ complex was investigated both in the solid state and in solution, by structural, spectroscopic, electrochemical, and magnetic methods. In the solid state, the cobalt ion of this dinuclear complex exhibits a spin crossover involving a $[\text{Fe}_{\text{LS}}^{\text{III}}\text{-CN-Co}_{\text{LS}}^{\text{II}}]$ ground state and a thermally populated

[Fe_{LS}^{III}-CN-Co_{HS}^{II}] state. The possible electron transfer process could be ruled out through variable temperature detailed crystallographic studies, magnetic measurements and ⁵⁷Fe Mössbauer spectroscopy. To our knowledge, this compound is the only example of a heterobimetallic complex exhibiting a spin crossover on a cobalt ion. Remarkably, our studies in solution reveal important optical and magnetic changes induced by an intramolecular metal-to-metal electron transfer triggered and modulated by a controlled protonation of the complex. Therefore, the [FeCo] molecule acts as two different molecular switches depending on its physical state and external stimuli: spin crossover in solid-state induced by temperature, and intramolecular electron transfer in solution assisted by protonation. This dual property for a single complex is unprecedented and represents a new contribution to the emerging field of multifunctional tuneable molecular complexes.

Experimental section

Materials

The PY5Me₂ and H₂BBP ligands were prepared as previously reported.^{24,25} The synthesis of [Co(PY5Me₂)(OH₂)](BF₄)₂ and [(BBP)Fe(CN)₃Co(PY5Me₂)]·2.5CH₃OH were performed under an argon atmosphere using standard Schlenk and drybox techniques. Solvents for these reactions were degassed using freeze-pump-thaw method and kept under nitrogen.

Synthesis of (Bu₄N)₂[Fe(BBP)(CN)₃]·6H₂O (1)

H₂BBP (3.13 g, 10 mmol) in 20 mL of CH₃OH was added to a methanolic solution (60 mL) of FeCl₃·6H₂O (2.70 g, 10 mmol). The resulting red solution was refluxed for 1 h followed by addition of NaCN (3.00 mg, 60 mmol) in 20 mL of water. The mixture was refluxed for further 8 h during which time the solution changed to dark blue. The solvent was then removed on a rotary evaporator, the resulting blue solid was extracted with dry methanol. On addition of ether the solution formed a blue powder. Yield: 4.12 g (71%). To an aqueous solution (30 mL) of this blue powder (2.95 g, 5 mmol) was added tetrabutylammonium bromide (3.22 g, 10 mmol) in water (20 mL). The instantaneous blue precipitate was collected by filtration, washed with water and air-dried. The polycrystalline product was dissolved in a mixture of methanol and water, and sheet-like crystals of intense blue colour were obtained by slow evaporation. Yield: 4.37 g (89%); FT-IR (ATR, cm⁻¹): 2959 (m), 2872 (m), 2109 (s), 1648 (w), 1614 (w), 1574 (w), 1451 (m), 1352 (m), 1323 (m), 1271 (m), 1146 (w), 1075 (w), 1029 (w), 998 (w) 917 (w), 865 (w), 747 (s), 646 (w); elemental analysis calc. for C₅₄H₉₁FeN₁₀O₄ (1 - 2H₂O) C 64.8, H 9.2, N 14.0; found: C 64.2, H 8.6, N 14.8%; χ_T product at 300 K: 0.48 cm³ K mol⁻¹ (*S* = 1/2, *g* ≈ 2.26).

Synthesis of [Co(PY5Me₂)(OH₂)](BF₄)₂ (2)

To an acetonitrile solution (5 mL) of PY5Me₂ (200 mg, 0.45 mmol) was added a methanolic solution (5 mL) of Co(BF₄)₂·6H₂O (150 mg, 0.45 mmol). The pale orange coloured solution was stirred for 3 h, and then filtrated. The slow diffusion of ether vapour afforded yellow crystals. Yield 0.27 g (86%);

FT-IR (ATR, cm⁻¹): 3406 (m), 1644 (w), 1594 (s), 1470 (w), 1466 (m), 1454 (m), 1440 (m), 1411 (w), 1389 (w), 1067 (s), 1016 (s), 995 (s), 865 (w), 843 (w), 762 (m), 628 (m), 576 (w); elemental analysis calc. for C₂₉H₂₇B₂CoF₈N₅O (2): C 50.2, H 3.9, N 10.1; found: C 50.2, H 4.2, N 10.3%; χ_T product at 300 K: 2.62 cm³ K mol⁻¹ (*S* = 3/2, *g* ≈ 2.36).

Synthesis of [(BBP)Fe(CN)₃Co(PY5Me₂)]·2.5CH₃OH ([FeCo])

A methanolic solution (5 mL) of 1 (71 mg, 0.065 mmol) was layered with an acetonitrile solution (5 mL) of 2 (47 mg, 0.065 mmol) in a tube of 2 × 12 cm. Square-like single crystals suitable for X-ray diffraction were obtained after 1 week. Yield 51 mg (75%); FT-IR (ATR, cm⁻¹): 3337 (br), 2161 (w), 2137 (m), 2118 (m), 1642 (w), 1592 (m), 1507 (w), 1451 (m), 1439 (m), 1348 (m), 1320 (m), 1265 (m), 1057 (m), 1022 (s), 916 (m), 861 (m), 817 (m), 745 (s), 646 (m); elemental analysis calc. for C₅₂H₄₄CoFeN₁₃O₃ ([FeCo] - 1.5CH₃OH + 2H₂O): C 61.6, H 4.4, N 17.9; found: C 61.5, H 4.4, N 17.8%. It is also important to note that the experimental powder diffraction of [FeCo] at 298 K corresponds well to the simulated one from the single-crystal data at 270 K (see Fig. S7†). This result excludes the possibility of a mixture of different species responsible for the observed magnetic properties (see Fig. 2). Moreover, no proof of statistical structural disorder has been observed on the thermal ellipsoids of the atoms of the complex at 90 K (see Fig. S4†), demonstrating a full transformation of the Co coordination sphere during the spin crossover process in the material upon lowering the temperature.

Synthesis of [Fe(H₂BBP)(CN)₃]·H₂O (3)

To a methanolic solution (5 mL) of 1 (100 mg, 0.095 mmol) was added 2 eq. of trifluoroacetic acid (1.46 × 10⁻² mL, 0.19 mmol). The solution was slowly evaporated to give dark violet crystals. More than 2 eq. of acid up to 10 eq. of acid afforded identical crystals. Yield 38 mg (86%); FT-IR (ATR, cm⁻¹) 2119 (w), 1783 (s), 1592 (w), 1468 (w), 1387 (m), 1352 (m), 1178 (m), 1117 (m), 1047 (m), 845 (m), 775 (m), 755 (m), 710 (m) 571 (w), 561 (w); elemental analysis calc for C₂₂H₁₅FeN₈O: C 57.0, H 3.3, N 24.2; found: C 56.8, H 3.0, N 23.9%.

Physical measurements

Elemental analysis. Elemental analysis was performed on a Thermo Fischer Flash EA 1112 equipment.

FT-IR spectra. FT-IR spectra were recorded in the range 400–4000 cm⁻¹ on a Thermal Scientific Nicolet 6700 ATR (attenuated total reflection) spectrometer equipped with a smart iTR diamond window.

Single crystal X-ray. Single crystal X-ray data were collected on single crystals mounted in Paratone-N oil on a 50 μm MicroMounts™ rod. The crystallographic data were collected with a Bruker APEX II diffractometer, equipped with a graphite monochromator centred on the path of Mo K_α. The program SAINT was used to integrate the data, which was thereafter corrected for absorption using SADABS.³³ All structures were solved by direct methods and refined by a full-matrix least-squares method on F² using SHELXL97.³⁴ Hydrogen atoms were placed at calculated positions using suitable riding models,

except those belonging to the coordinated water molecule in compound 2 and those connected to the nitrogen atoms in compound 3. The latter were found in the difference Fourier maps, and refined using DFIX constraints in compound 3. All hydrogen atoms were refined using isotropic displacement parameters derived from their parent atoms. Non-hydrogen atoms were refined with anisotropic displacement parameters.

Magnetic susceptibility measurements. Magnetic susceptibility measurements were carried out on a Quantum Design SQUID magnetometer MPMS-XL operating between 1.8 and 400 K for applied dc fields ranging from -70 kOe to 70 kOe. An M vs. H measurement was performed at 100 K to confirm the absence of ferromagnetic impurities. Experimental data were corrected for the sample holder and for the diamagnetic contribution of the sample.

Mössbauer measurements. Mössbauer measurements were performed using a constant acceleration HALDER-type spectrometer with a room temperature $^{57}\text{Co}/\text{Rh}$ source in transmission geometry. The polycrystalline absorber containing about 10 mg cm^{-2} of iron was used to avoid experimental broadening of the peaks. The spectra were recorded at 293 and 4.2 K using a variable temperature cryostat. The velocity was calibrated using pure iron metal as the standard material. The refinement of Mössbauer spectra has been done assuming a distribution of hyperfine fields. It is worth mentioning that the small difference on the isomer shift depending on the temperature is due to the relativistic second order Doppler shift.

Thermogravimetric analysis. The thermogravimetric analysis (TGA) was carried out between 298 and 900 K at 5 K min^{-1} in a nitrogen atmosphere using a thermogravimetric analyser Setaram TAG 16.

Powder X-ray diffraction. Powder X-ray diffraction patterns were recorded at 298 K on a PANalytical X'pert MPD Bragg-Brentano θ - θ geometry diffractometer equipped with a secondary monochromator over an angular range of $2\theta = 8$ – 30° . The Cu K_α radiation was generated at 40 kV and 40 mA. The samples were put on sample holders made of silicon and flattened with a piece of glass.

UV-vis spectra. UV-vis spectra were collected between 400 and 900 nm using a UNICAM UV4-100 Spectrophotometer.

NMR spectra. NMR spectra were obtained with JEOL JMN-ECS 400 system.

Cyclic voltammetry measurements. Cyclic voltammetry measurements were carried out in a standard one-compartment cell under N_2 , equipped with platinum wires for counter/working electrodes and silver wire for reference electrode using a CHI 760c potentiostat. The measurements were performed in dimethylsulfoxide (for 1, 3 and $[\text{FeCo}]$) and in acetonitrile (for 2) with 0.1 M tetrabutylammonium hexafluorophosphate ($[\text{Bu}_4\text{N}^+][\text{PF}_6^-]$) as the supporting electrolyte.

Spectroelectrochemical measurements. Spectroelectrochemical measurements were carried out in an OTTL cell (purchased from the University of Reading, UK)³⁵ with CaF_2 windows separated by a $200\text{ }\mu\text{M}$ PE spacer embedding Pt grids as working and counter electrodes and an Ag/AgCl wire as a pseudoreference electrode, using a Metrohm PGSTAT101 potentiostat. Spectra were collected between 400 and 1000 nm using a Varian

Cary 5 spectrophotometer. Measurements were performed in identical conditions (solvent, electrolyte type and concentration). Electrolyses were performed at fixed potential, monitoring the decrease of the current, before spectra acquisition.

Acknowledgements

This work was supported by the University of Bordeaux, the CNRS, the ANR (NT09_469563, AC-MAGnets), the Région Aquitaine, the GIS Advanced Materials in Aquitaine (COMET Project) and the Institut Universitaire de France (IUF). We acknowledge Stéphane Baudron, Philippe Guionneau, Nicolas Mano, Eric Lebraud, Fabien Durola, Stephen Holmes, Dongfeng Li and Guillem Aromi for fruitful discussions and advice.

Notes and references

‡ The following equation deduced from the ideal solution model²⁹ was used to fit the spin crossover behaviour observed by magnetic measurements, with X being the χT product, X_{LS} and X_{HS} being the χT products for pure low-spin and high-spin

$$X = X_{\text{LS}} + \frac{X_{\text{HS}} - X_{\text{LS}}}{1 + \exp\left(\frac{\Delta H}{R} \left(\frac{1}{T} - \frac{1}{T_{1/2}}\right)\right)}$$

species, respectively, ΔH being the enthalpy change associated to the spin crossover phenomenon and R being the ideal gas constant.

§ The theoretical susceptibility deduced from the Heisenberg dinuclear isotropic $S = 1/2$ spin Hamiltonian ($H = -2J S_{\text{Co}} S_{\text{Fe}}$) was calculated from the van Vleck equation in the weak field approximation.

$$\chi T = \frac{2N\mu_{\text{B}}^2 g^2}{k_{\text{B}}} \frac{1}{3 + \exp(-2J/k_{\text{B}}T)}$$

¶ Even if the nitrogen atom of the $\text{Fe}(\text{III})$ precursor cyanide is likely a better donor group to the $\text{Co}(\text{II})$ ion than the oxygen atom of DMSO, the stability of the neutral $[\text{FeCo}]$ in DMSO solutions was checked by combined techniques: UV-vis spectroscopy, cyclic voltammetry and NMR. The UV-vis measurements (Figs. 4, S10 and S19†) show that the LMCT band for the $\{[\text{BBP}]\text{Fe}^{\text{III}}(\text{CN})_3\}$ part of $[\text{FeCo}]$ is clearly shifted by about 1300 cm^{-1} , suggesting the absence of free $[[\text{BBP}]\text{Fe}^{\text{III}}(\text{CN})_3]^{2-}$ precursor in DMSO solution and its full coordination. The $\text{Fe}^{\text{III}}/\text{Fe}^{\text{II}}$ redox potential observed for the $[[\text{BBP}]\text{Fe}^{\text{III}}(\text{CN})_3]^{2-}$ precursor at -1.09 V (Fig. S16†) is shifted significantly by $+0.18\text{ V}$ for the $[\text{FeCo}]$ complex (Fig. 6). Similar effects upon coordination have already been seen in several dinuclear Co/Fe cyanido-bridged complexes reported by Bernhardt *et al.*^{13–15} that show positive shifts between $+0.17$ and 0.20 V in perfect agreement with the present results for $[\text{FeCo}]$. The NMR spectrum shown in Fig. 5a for a DMSO solution of the $[\text{FeCo}]$ complex is completely different from a simple superposition of the NMR spectra of the precursors in DMSO shown in Fig. S11.† Therefore, the dinuclear $[\text{FeCo}]$ complex is stable in DMSO solution without significant dissociation at room temperature.

- O. Sato, T. Iyoda, A. Fujishima and K. Hashimoto, *Science*, 1996, **272**, 704–705.
- O. Sato, J. Tao and Y.-Z. Zhang, *Angew. Chem., Int. Ed.*, 2007, **46**, 2152–2187.
- C. Simão, M. Mas-Torrent, N. Crivillers, V. Lloveras, J. M. Artés, P. Gorostiza, J. Veciana and C. Rovira, *Nat. Chem.*, 2011, **3**, 359–364.
- F. Prins, M. Monrabal-Capilla, E. A. Osorio, E. Coronado and H. S. J. van der Zant, *Adv. Mater.*, 2011, **23**, 1545–1549.
- A. Bleuzen, C. Lomenech, V. Escax, F. Villain, F. Varret, C. Cartier dit Moulin and M. Verdagner, *J. Am. Chem. Soc.*, 2000, **122**, 6648–6652.

- 6 S.-i. Ohkoshi, H. Tokoro, T. Hozumi, Y. Zhang, K. Hashimoto, C. Mathonière, I. Bord, G. Rombaut, M. Verelst, C. Cartier dit Moulin and F. Villain, *J. Am. Chem. Soc.*, 2006, **128**, 270–277.
- 7 S.-i. Ohkoshi, Y. Hamada, T. Matsuda, Y. Tsunobuchi and H. Tokoro, *Chem. Mater.*, 2008, **20**, 3048–3054.
- 8 H. Tokoro, T. Matsuda, T. Nuida, Y. Moritomo, K. Ohoyama, E. D. L. Dangui, K. Boukheddaden and S.-i. Ohkoshi, *Chem. Mater.*, 2008, **20**, 423–428.
- 9 C. Avendano, M. G. Hilfiger, A. Prosvirin, C. Sanders, D. Stepien and K. R. Dunbar, *J. Am. Chem. Soc.*, 2010, **132**, 13123–13125.
- 10 N. Ozaki, H. Tokoro, Y. Hamada, A. Namai, T. Matsuda, S. Kaneko and S.-i. Ohkoshi, *Adv. Funct. Mater.*, 2012, **22**, 2089–2093.
- 11 C. P. Berlinguette, A. Dragulescu-Andrasi, A. Sieber, J. R. Galán-Mascarós, H.-U. Güdel, C. Achim and K. R. Dunbar, *J. Am. Chem. Soc.*, 2004, **126**, 6222–6223.
- 12 C. P. Berlinguette, A. Dragulescu-Andrasi, A. Sieber, H.-U. Güdel, C. Achim and K. R. Dunbar, *J. Am. Chem. Soc.*, 2005, **127**, 6766–6779.
- 13 P. V. Bernhardt and M. Martinez, *Inorg. Chem.*, 1999, **38**, 424–425.
- 14 P. V. Bernhardt, B. P. Macpherson and M. Martinez, *Inorg. Chem.*, 2000, **39**, 5203–5208.
- 15 P. V. Bernhardt, B. P. Macpherson and M. Martinez, *J. Chem. Soc., Dalton Trans.*, 2002, 1435–1441.
- 16 H. Oshio, H. Onodera, O. Tamada, H. Mizutani, T. Hikichi and T. Ito, *Chem.–Eur. J.*, 2000, **6**, 2523–2530.
- 17 D. Li, R. Clérac, O. Roubeau, E. Harté, C. Mathonière, R. Le Bris and S. M. Holmes, *J. Am. Chem. Soc.*, 2008, **130**, 252–258.
- 18 Y. Zhang, D. Li, R. Clérac, M. Kalisz, C. Mathonière and S. M. Holmes, *Angew. Chem., Int. Ed.*, 2010, **49**, 3752–3756.
- 19 J. Mercuriol, Y. Li, E. Pardo, O. Risset, M. Seuleiman, H. Rousselière, R. Lescouëzec and M. Julve, *Chem. Commun.*, 2010, **46**, 8995–8997.
- 20 M. Nihei, Y. Sekine, N. Suganami, K. Nakazawa, A. Nakao, H. Nakao, Y. Murakami and H. Oshio, *J. Am. Chem. Soc.*, 2011, **133**, 3592–3600.
- 21 D. Siretanu, D. Li, L. Buisson, D. M. Bassani, S. M. Holmes, C. Mathonière and R. Clérac, *Chem.–Eur. J.*, 2011, **17**, 11704–11708.
- 22 T. Liu, D.-P. Dong, S. Kanegawa, S. Kang, O. Sato, Y. Shiota, K. Yoshizawa, S. Hayami, S. Wu, C. He and C.-Y. Duan, *Angew. Chem., Int. Ed.*, 2012, **51**, 4367–4370.
- 23 M. Nihei, Y. Yuki, Y. Sekine, N. Hoshino, T. Shiga, I. P.-C. Liu and H. Oshio, *Angew. Chem., Int. Ed.*, 2012, **51**, 6361–6364.
- 24 B. Bechlars, D. M. D'Alessandro, D. M. Jenkins, A. T. Iavarone, S. D. Glover, C. P. Kubiak and J. R. Long, *Nat. Chem.*, 2010, **2**, 362–368.
- 25 (a) A. W. Addison and P. J. Burke, *J. Heterocycl. Chem.*, 1981, **18**, 803–805; (b) A. Panja, P. Guionneau, I.-R. Jeon, S. M. Holmes, R. Clérac and C. Mathonière, *Inorg. Chem.*, 2012, **51**, 12350–12359.
- 26 J. Zarembowitch, *New J. Chem.*, 1992, **16**, 255–267; H. A. Goodwin, *Top. Curr. Chem.*, 2004, **234**, 23–47; I. Krivokapic, M. Zerara, M. L. Daku, A. Vargas, C. Enachescu, C. Ambrus, P. Tregenna-Piggott, N. Amstutz, E. Krausz and A. Hauser, *Coord. Chem. Rev.*, 2007, **251**, 364–378.
- 27 P. E. Figgins and D. H. Busch, *J. Am. Chem. Soc.*, 1960, **82**, 820–824; R. C. Stoufer, D. H. Busch and W. B. Hadley, *J. Am. Chem. Soc.*, 1961, **83**, 3732–3734; R. Hogg and R. G. Wilkins, *J. Chem. Soc.*, 1962, 341; C. L. Raston and A. H. White, *J. Chem. Soc., Dalton Trans.*, 1976, 7–12; S. Kremer, W. Henke and D. Reinen, *Inorg. Chem.*, 1982, **21**, 3013–3022; B. N. Figgis, E. S. Kucharski and A. H. White, *Aust. J. Chem.*, 1983, **36**, 1537–1561; J. A. Wolny, M. F. Rudolf, Z. Ciunik, K. Gatner and S. Wolowicz, *J. Chem. Soc., Dalton Trans.*, 1993, 1611–1621; K. Heinze, G. Huttner, L. Zsolnai and P. Schober, *Inorg. Chem.*, 1997, **36**, 5457–5469; A. B. Gaspar, M. C. Munoz, V. Niel and J. A. Real, *Inorg. Chem.*, 2001, **40**, 9–10; S. Hayami, Y. Shigeyoshi, M. Akita, K. Inoue, K. Kato, K. Osaka, M. Takata, R. Kawajiri, T. Mitani and Y. Maeda, *Angew. Chem., Int. Ed.*, 2005, **44**, 4899–4903; D. Schweinfurth, F. Weisser, D. Bubrin, L. Bogani and B. Sarkar, *Inorg. Chem.*, 2011, **50**, 6114–6121.
- 28 B. Fultz, in *Characterization of Materials (part of Mössbauer Spectrometry)*, ed. E. Kaufmann, John Wiley, New York, 2011.
- 29 P. Atkins and J. De Paula, *Physical Chemistry*, Oxford University Press, 2006, ch. 5.
- 30 (a) A. B. P. Lever, *Inorganic Electronic Spectroscopy*, Elsevier Science, 1985; (b) D. Li, S. Parkin, G. Wang, G. T. Yee and S. M. Holmes, *Inorg. Chem.*, 2006, **45**, 1951–1959; (c) G. M. Bryant, J. E. Fergusson and H. K. J. Powell, *Aust. J. Chem.*, 1971, **24**, 257–273; (d) R. R. Ruminski and J. L. Kiplinger, *Inorg. Chem.*, 1990, **29**, 4581–4584.
- 31 P. V. Bernhardt, F. Bozoglian, B. P. Macpherson, M. Martínez, G. González and B. Sienra, *Eur. J. Inorg. Chem.*, 2003, **13**, 2512–2518.
- 32 I. Ratera, C. Sporer, D. Ruiz-Molina, N. Ventosa, J. Baggerman, A. M. Brouwer, C. Rovira and J. Veciana, *J. Am. Chem. Soc.*, 2007, **129**, 6117–6129.
- 33 G. M. Sheldrick, *SADABS, version 2.03*, Bruker Analytical X-Ray Systems, Madison, WI, 2000.
- 34 G. M. Sheldrick, *SHELXL97, Program for Crystal Structure Refinement*, University of Göttingen, 1997.
- 35 M. Krejčík, M. Danek and F. Hartl, *J. Electroanal. Chem.*, 1991, **317**, 179–187.